Energy Stable SBP-FDTD Methods for Maxwell–Duffing Models in Nonlinear Photonics

Daniel Appelö, Vrushali A. Bokil, Yingda Cheng, and Fengyan Li

***Abstract*—We consider electromagnetic models that describe nonlinear optical phenomenon in which the nonlinear polarization is driven by the electric field and modeled as anharmonic oscillator(s). These models are given by *Duffing equations* and incorporate both nonlinearity and dispersion. Using the auxiliary differential equation approach, our discretizations of the coupled Maxwell–Duffing models are high-order and energy-stable finite-difference time-domain (FDTD) methods of so-called summation by parts (SBP) type. Boundary and interface conditions are handled by the simultaneous approximation technique (SAT).**

***Index Terms*—Kerr effect, Maxwell–Duffing, nonlinear photonics, simultaneous approximation term (SAT), summation by parts (SBP).**

I. Introduction

ACCURATE, stable, and efficient simulation of wave propagation in optical media is becoming increasingly important as high-power lasers become more common both in the laboratory and industrial setting. It is well known that high-order accurate methods are more computationally efficient than low (second order and below)-order accurate methods to achieve high resolution in many applications. Despite this fact, it is still very common to use the Yee finite-difference time-domain (FDTD) scheme for electromagnetic computations. A reason for the persisting popularity of the Yee-FDTD scheme is its simplicity, combined with its ability to preserve energy on the discrete grid.

In this article, we consider energy-stable, staggered, and nonstaggered finite-difference discretizations of Maxwell's equations in a nonmagnetic dispersive nonlinear optical medium using summation by parts (SBP) operators [1]. Using the auxiliary differential equation (ADE) technique [2], we append to Maxwell's equations constitutive laws involving ordinary differential equations (ODEs) that model the time evolution of the macroscopic polarization (average dipole moment per unit volume). In particular, the nonlinearity appears in the constitutive laws due to the response of the medium to the incident electromagnetic fields, and is only present in the ODEs for the time evolution of the polarization. The polarization models that we consider below, called Duffing models, only contain nonlinearity in the zeroth-order term, and we can directly apply to these models the SBP methods developed by Nordström and Gustafsson for Maxwell's equations in linear and nondispersive materials [3]. We show that our adaptations to the Maxwell–Duffing nonlinear model are also high order, energy stable, and conserve a discrete version of the continuous energy of the nonlinear physical system.

We derive the energy analysis of the SBP method for the semidiscrete system only. In order to preserve a fully discrete energy and in order to achieve a uniformly high-order method, time integrators need to be chosen carefully. We note that the second-order accurate fully discrete energy stable time discretizations, that we derived in [4], could also be applied to the Maxwell–Duffing models in conjunction with the spatial discretization considered here. In this article, however, we consider both explicit Runge–Kutta and Taylor methods, as well as implicit Runge–Kutta methods based on Gauss–Legendre quadrature. The use of Gauss–Legendre quadrature makes the resulting (collocation) Runge–Kutta method symplectic. Of course, there is no guarantee that a symplectic method will preserve energy exactly (although a nearby energy will be preserved), so we settle for solving the nonlinear system of equations approximately using the so-called spectral deferred correction (SDC) method [5], [6]. In SDC, the nonlinear system is turned into a fixed point iteration. If the fixed point is found to machine precision, then the SDC solution is the same as the (symplectic) Runge–Kutta solution, but if the iteration is terminated based on order-of-accuracy consideration, the symplectic property is only approximately satisfied. Despite this approximation and the fact that symplecticity does not imply energy conservation, we demonstrate through numerical examples that (at least for the models considered here) very good energy conservation properties are attainable when SDC methods are used.

To model nonlinearity and dispersion in optical phenomenon, we consider a general class of polarization models called *Duffing equations* [7]. Historically, the Duffing equation, which is named after Georg Duffing, is a nonlinear second-order ODE modeling the free and forced harmonic vibration of an oscillator in which the stiffness force has quadratic and cubic terms [8].

Manuscript received September 6, 2019; revised November 11, 2019; accepted December 2, 2019. Date of publication December 13, 2019; date of current version January 9, 2020. This work was supported in part by the National Science Foundation under Grant NSF-1913076 (PI Appelö), Grant NSF-1720116 (PI Bokil), Grant NSF-1453661, and Grant NSF-1720023 (PI Cheng), and Grant NSF-1719942 and Grant DMS-1913072 (PI Li). *(Corresponding author: Daniel Appelo.)*

D. Appelö is with the Department of Applied Mathematics, University of Colorado Boulder , Boulder, CO 80309 USA (e-mail: daniel.appelo@colorado.edu).

V. A. Bokil is with the Department of Mathematics, Oregon State University, Corvallis, OR 97331 USA (e-mail: bokilv@math.oregonstate.edu).

Y. Cheng is with the Department of Mathematics, Department of Computational Mathematics, Science and Engineering, Michigan State University, East Lansing, MI 48824 USA (e-mail: ycheng@msu.edu).

F. Li is with the Department of Mathematical Sciences, Rensselaer Polytechnic Institute, Troy, NY 12180 USA (e-mail: lif@rpi.edu).

Digital Object Identifier 10.1109/JMMCT.2019.2959587

Subsequently, the label *Duffing equation* has been used to describe any oscillator that has a cubic stiffness term, regardless of the type of damping or excitation [8]. In nonlinear optics, Duffing equations are used to model the polarization accounting for dispersion and nonlinearity related to third-order effects in optical and photonic materials. These equations include the finite and retarded response time of the medium and are advantageous in studying the propagation characteristics of ultrashort laser pulses [9]. In this article, we consider a variety of Maxwell–Duffing models and their discretizations by the SBP methods to simulate nonlinear optical phenomenon. In particular, we present the construction of high-order-in-space SBP methods and simultaneous approximation terms, along with high-order time discretizations, and we demonstrate the effectiveness of our new discretizations on a variety of test problems.

The rest of the article is organized as follows. In Section II, we introduce the models for simulating nonlinear optical phenomenon, and in Section III, we describe the numerical discretizations. In Section IV, numerical experiments are reported. Section V concludes the article.

II. Models and Constitutive Laws for Nonlinear Optical Materials

To observe nonlinear effects in common materials, high-intensity light sources, such as lasers, are required, and the particular nonlinear effects observed depend on which term is dominant in the electric polarization [10]. We will consider materials in which the dominant nonlinearities are of the third order (such as optical glass fibers) and include instantaneous as well as delayed material responses.

Using the ADE approach, we append to Maxwell's partial differential equations (PDEs) a system of ODEs describing the nonlinear relationship between the macroscopic polarization vector field $\mathbf{P}$ and the electric field $\mathbf{E}$. Our approach follows the development in [11]. The hybrid system of Maxwell PDEs and auxiliary ODEs are then simultaneously evolved in time.

Maxwell's equations in a nonmagnetic, nonconductive medium $\Omega \subset \mathbb{R}^d, d = 1, 2, 3,\ T > 0$, containing no free charges, govern the dynamic evolution of the electric field $\mathbf{E}$ and the magnetic field $\mathbf{H}$. The evolution equations are

$$\mu_0 \partial_t \mathbf{H} + \nabla \times \mathbf{E} = 0, \text{ in } (0, T] \times \Omega \tag{1a}$$

$$\epsilon_0 \epsilon_\infty \partial_t \mathbf{E} + \epsilon_0 \mathbf{J} - \nabla \times \mathbf{H} = 0, \text{ in } (0, T] \times \Omega \tag{1b}$$

$$\nabla \cdot \mathbf{B} = 0,\ \nabla \cdot \mathbf{D} = 0, \text{ in } (0, T] \times \Omega \tag{1c}$$

The electric flux density $\mathbf{D}$, and the magnetic induction $\mathbf{B}$, are related to the electric field and magnetic field, respectively, via the constitutive laws

$$\mathbf{D} = \epsilon_0(\epsilon_\infty \mathbf{E} + \mathbf{P}),\ \ \mathbf{B} = \mu_0 \mathbf{H} \tag{2}$$

with the polarization current density, $\mathbf{J}$, defined as the time derivative of the macroscopic polarization, i.e., $\mathbf{J} = \partial_t \mathbf{P}$. The parameter ϵ_0 is the electric permittivity of free space, while μ_0 is the magnetic permeability of free space. The term $\epsilon_\infty \mathbf{E}$ captures the linear instantaneous response of the material to the EM fields, with ϵ_∞ defined as the relative electric permittivity in the limit of infinite frequencies. The macroscopic *(electric) polarization* $\mathbf{P}$ includes both linear and nonlinear effects, and is related to the electric field through different mechanisms depending on the optical phenomenon under consideration. In this work, we focus on *general Maxwell–Duffing dispersive models.*

The Duffing equation, for the electric polarization, models high-order effects by including both nonlinearity and dispersion, and can be written in a general form as

$$\frac{\partial^2 \mathbf{P}}{\partial t^2} + \frac{1}{\tau}\frac{\partial \mathbf{P}}{\partial t} + \omega_0^2 \mathbf{P} F(\mathbf{P}) = \omega_p^2 \mathbf{E} \tag{3}$$

with a range of choices for $F(\mathbf{P})$. Here ω_0 and ω_p are the resonance and plasma frequencies of the medium, respectively, and τ^{-1} is a damping constant. In this article, we will consider an *N*th-order polynomial model for the Duffing equation, given as

$$F(\mathbf{P}) = F_{\mathrm{PMD}}(\mathbf{P}) := \sum_{l=0}^{N_{\mathrm{PMD}}} \lambda_{2l} |\mathbf{P}|^{2l} \tag{4}$$

with $N_{\mathrm{PMD}} \in \mathbb{N}, N_{\mathrm{PMD}} \geq 1$. We refer to the system of equations (1)–(4) as the *Nth Order polynomial Maxwell–Duffing (PMD) model*. This includes as special cases the *cubic-exponential Maxwell–Duffing (C-EMD)* model ($N_{\mathrm{PMD}} = 1, \lambda_0 = 1,\ \lambda_2 = \alpha$), the *quintic-exponential Maxwell–Duffing (Q-EMD)* model ($N_{\mathrm{PMD}} = 2, \lambda_0 = 1,\ \lambda_2 = \alpha,\ \lambda_4 = \alpha^2/2$), and in general an *Nth-order polynomial exponential Maxwell–Duffing (P-EMD) model* which are all approximations of the *exponential Maxwell–Duffing (EMD)* model with $F(\mathbf{P}) := \exp(\alpha |\mathbf{P}|^2)$.

We note that the PMD model is more general in that it incorporates the C-EMD, Q-EMD, and higher order approximations P-EMD of the EMD, but can also be used with other parameters, λ_{2l}, that are not approximations of the EMD, as is suggested by our energy estimates below.

We note that if $F(\mathbf{P}) = 1$, the Duffing model reduces to the linear Lorentz dispersive model. On the other hand, as pointed out in [12], for a specific function form [different than (4)] of $F(\mathbf{P})$, under certain assumptions, the Duffing model (3) will reproduce the Kerr model, another widely used nonlinear model to describe cubic nonlinear effects such as the Kerr effect [13]. We refer the reader to our recent work [14], on the construction of energy stable FDTD approximations of Maxwell's equations along with the nonlinear Kerr–Raman model for polarization.

The Maxwell–Duffing models need to be closed by initial and boundary conditions on $[0, T] \times \Omega$. Here we will exclusively consider perfect electric conductors (PEC) resulting in homogeneous Dirichlet boundary conditions on the tangential components of the electric field on $\partial\Omega$, the boundary of the domain Ω.

A. Energy Estimate in Two Dimensions

In two dimensions, assuming a transverse electric mode, the electric field, $\mathbf{E} = (E^x, E^y)$, and polarization, $\mathbf{P} = (P^x, P^y)$, have two components each that are incident in the (x, y) plane, while the magnetic field has one component, H^z, transverse to the electric field out of this plane. Using the polarization current

density $\mathbf{J} = (J^x, J^y)$, and assuming the Duffing model (3) to be damping-free ($\tau^{-1} = 0$), we rewrite (3) in first-order form as

$$\frac{\partial \mathbf{J}}{\partial t} = -\omega_0^2 \mathbf{P} F_{\mathrm{PMD}}(\mathbf{P}) + \omega_p^2 \mathbf{E}. \tag{5}$$

We assume the PEC boundary conditions for the electric field on $\partial\Omega$. An energy identity for this model can be obtained using the energy method as follows. Multiplying (5) by ε_0/ω_p^2, multiplying each equation in (1a), (1b), and (5) by appropriate quantities and summing over the domain, taking norms, together with integration by parts in (1b), we obtain the energy identity

$$\frac{1}{2}\frac{d}{dt}\mathcal{E}(t) = 0 \tag{6}$$

where, the time-dependent *energy* of the PDM model denoted as $\mathcal{E}(t)$ is defined as

$$\mathcal{E}(t) := \mu_0 \|H^z\|^2 + \varepsilon_0\varepsilon_\infty \|\mathbf{E}\|^2 + \frac{\varepsilon_0}{\omega_p^2}\|\mathbf{J}\|^2 + \frac{\varepsilon_0\omega_0^2}{\omega_p^2}\sum_{l=0}^{N\mathrm{PMD}} \frac{\lambda_{2l}}{1+l}(\|\mathbf{P}\|^2)^{1+l}. \tag{7}$$

Equation (6) implies that the energy $\mathcal{E}$ is constant in time. Here $\|\cdot\|$ is the standard L_2 norm with respect to the spatial domain, induced by the standard L_2 inner product $(\cdot,\cdot)$. Note that the damped case can be treated analogously but that $\mathcal{E}'(t) \leq 0$ in the presence of damping ($\tau^{-1} \neq 0$.)

III. Numerical Methods

A. Summation by Parts (SBP) Finite Difference Methods

The main idea behind summation by parts finite differences is to design difference approximations that mimic the integration by parts formula, which in one dimension on $[x_L, x_R] \subset \mathbb{R}$, can be written as

$$\int_{x_L}^{x_R} u(x)v_x(x)dx = -\int_{x_L}^{x_R} u_x(x)v(x)dx + u(x_R)v(x_R) - u(x_L)v(x_L) \tag{8}$$

so that the energy analysis of the continuous problem can be directly applied to the semidiscretization (in space) of the governing equations at hand.

As an illustrative example of deriving an energy identity, consider the 1-D linear version of the PMD model with $N_{\mathrm{PMD}} = 0, \lambda_0 = 1$, governing the electric and magnetic fields, E and H, in a nonmagnetic dispersive optical medium. From (1)–(3), we have the following 1-D model:

$$\varepsilon_0\varepsilon_\infty E_t = H_x - \varepsilon_0 J \tag{9a}$$

$$\mu_0 H_t = E_x \tag{9b}$$

$$P_t = J \tag{9c}$$

$$J_t = -J/\tau - \omega_0^2 P + \omega_p^2 E. \tag{9d}$$

Following similar steps as in the 2-D case above we arrive at an energy identity. In particular, multiplying the above equations by suitable quantities and integrating over the domain Ω, we obtain the equations

$$(\varepsilon_0\varepsilon_\infty E, E_t) = (E, H_x) - \varepsilon_0(E, J)$$

$$(\mu_0 H, H_t) = (H, E_x)$$

$$\frac{\varepsilon_0\omega_0^2}{\omega_p^2}(P, P_t) = \frac{\varepsilon_0\omega_0^2}{\omega_p^2}(P, J)$$

$$\frac{\varepsilon_0}{\omega_p^2}(J, J_t) = -\frac{\varepsilon_0}{\omega_p^2\tau}(J, J) - \frac{\varepsilon_0\omega_0^2}{\omega_p^2}(J, P) + \epsilon_0(J, E).$$

Summing up these equations we have

$$\frac{1}{2}\frac{d}{dt}\left(\varepsilon_0\varepsilon_\infty\|E\|^2 + \mu_0\|H\|^2 + \frac{\varepsilon_0\omega_0^2}{\omega_p^2}\|P\|^2 + \frac{\varepsilon_0}{\omega_p^2}\|J\|^2\right) = (E, H_x) + (E_x, H) - \frac{\varepsilon_0}{\omega_p^2\tau}\|J\|^2 = [EH]_{x_{\mathrm{L}}}^{x_{\mathrm{R}}} - \frac{\varepsilon_0}{\omega_p^2\tau}\|J\|^2.$$

Here the last equality follows from an integration by parts (IBP) in either of the terms $(E, H_x), (E_x, H)$.

The above energy estimate implies that, given suitable boundary conditions on E and H (for example $E = 0$ on the boundary), the initial boundary value problem is well-posed, i.e., the solution depends continuously on data (see, e.g., [15]).

Finite difference operators with the SBP property satisfy a discrete version of the continuous IBP formula (8). Precisely, given vector approximations $E^h, H^h \in \mathbb{R}^{n+1}$ to E and H, defined on a grid $x_i = x_{\mathrm{L}} + ih$, $i = 0, \ldots, n$, $h = (x_{\mathrm{R}} - x_{\mathrm{L}})/n$, *SBP operators for the first derivatives* $D \equiv R^{-1}Q$ are constructed so that

$$(E^h)^T RDH^h + (H^h)^T RDE^h = E_n^h H_n^h - E_0^h H_0^h.$$

Here R is a diagonal and positive definite matrix defining an inner product (and the induced norm), Q is a matrix with the property $Q + Q^T = e_n e_n^T - e_0 e_0^T$, with e_j being the jth unit vector. For the actual construction of SBP operators, we refer readers to the original paper by Kreiss and Scherer [16], and the paper by Strand [17], that contain many of the early operators and the more recent review by Svärd and Nordström [1]. Here, we simply assume that SBP operators exist. Next, we illustrate how these SBP operators can be used to simulate nonlinear optics problems in an accurate and stable manner.

The energy analysis is not changed by lower order terms. Thus, we illustrate the semidiscrete energy analysis using SBP operators for the linear 1-D problem (9) by suppressing the lower order terms in (9a). Using an SBP operator D to approximate $\partial/\partial x$, we obtain

$$\varepsilon_0\varepsilon_\infty E_t^h = DH^h \tag{10}$$

$$\mu_0 H_t^h = DE^h \tag{11}$$

to approximate (9a) and (9b). Multiplying the above equations by $(E^h)^T R$ and $(H^h)^T R$, respectively, followed by adding the resulting equations we find

$$\frac{1}{2}\frac{d}{dt}\left(\varepsilon_0\varepsilon_\infty\|E^h\|_R^2 + \mu_0\|H^h\|_R^2\right) = E_n^h H_n^h - E_0^h H_0^h.$$

The above equality illustrates that the change of energy is controlled by the approximations to the electric and magnetic fields

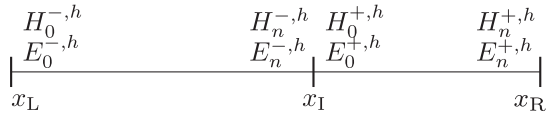

Fig. 1. Schematic of a two block computational domain. The blocks occupy $x \in [x_{\mathrm{L}}, x_{\mathrm{I}}]$ and $x \in [x_{\mathrm{I}}, x_{\mathrm{R}}]$. The continuity of the fields and the PEC boundary conditions are weakly enforced by SAT terms.

on the boundary. Below we discuss how to chose penalty terms to handle interface coupling and physical boundary conditions. A schematic of the computational setup can be found in Fig. 1.

1) Interfaces: Consider an interface between two grids with $E^{+,h}, H^{+,h}, E^{-,h}, H^{-,h}$ denoting the approximations to the right and to the left of the interface. To couple the two domains, we add "zeros," so-called *simultaneous approximation terms* (SATs), [18], to the approximation of the governing equations.

Focusing only on the terms near the interface the scheme takes the form

$$\begin{aligned}
\varepsilon_0^- \varepsilon_\infty^- E_t^{-,h} &= DH^{-,h} - \gamma R^{-1} e_n \left(H_n^{-,h} - H_0^{+,h} \right) \\
\mu_0^- H_t^{-,h} &= DE^{-,h} - (1-\gamma) R^{-1} e_n \left(E_n^{-,h} - E_0^{+,h} \right) \\
\varepsilon_0^+ \varepsilon_\infty^+ E_t^{+,h} &= DH^{+,h} + (1-\gamma) R^{-1} e_0 \left(H_0^{+,h} - H_n^{-,h} \right) \\
\mu_0^+ H_t^{+,h} &= DE^{+,h} + \gamma R^{-1} e_0 \left(E_n^{+,h} - E_0^{-,h} \right).
\end{aligned}$$

Multiplying by $(E^{-,h})^T R, (H^{-,h})^T R, (E^{+,h})^T R, (H^{+,h})^T R$, respectively, and adding the resulting equations yields

$$\begin{aligned}
&\frac{1}{2}\frac{d}{dt} \sum_{s\in\{+,-\}} \left(\varepsilon_0^s \varepsilon_\infty^s \|E^{s,h}\|_R^2 + \mu_0^s \|H^{s,h}\|_R^2 \right) \\
&= -\gamma E_n^{-,h} \left(H_n^{-,h} - H_0^{+,h} \right) - (1-\gamma) H_n^{-,h} \left(E_n^{-,h} - E_0^{+,h} \right) \\
&\quad + (1-\gamma) E_0^{+h} \left(H_0^{+,h} - H_n^{-,h} \right) + \gamma H_0^{+h} \left(E_n^{+,h} - E_0^{-,h} \right) \\
&\quad + E_n^{-,h} H_n^{-,h} - E_0^{+,h} H_0^{+,h} = 0.
\end{aligned}$$

This shows that the energy is conserved for any choice of γ.

2) Boundary Conditions: Boundary conditions are easily imposed through the SAT. For example, if we want to enforce homogeneous boundary conditions on E to the right we can assume there is a material to the right and take $E_0^{+,h} = 0$ and $H_0^{+,h} = H_n^{-,h}$ in the formulas above.

3) Dissipative Methods: We finally note that energy dissipating methods can be obtained by adding terms of the form

$$\begin{aligned}
\varepsilon_0^- \varepsilon_\infty^- E_t^{-,h} &= \cdots - \beta R^{-1} e_n \left(E_n^{-,h} - E_0^{+,h} \right) \\
\mu_0^- H_t^{-,h} &= \cdots - \beta R^{-1} e_n \left(H_n^{-,h} - H_0^{+,h} \right) \\
\varepsilon_0^+ \varepsilon_\infty^+ E_t^{+,h} &= \cdots - \beta R^{-1} e_0 \left(E_0^{+,h} - E_n^{-,h} \right) \\
\mu_0^+ H_t^{+,h} &= \cdots - \beta R^{-1} e_0 \left(H_n^{+,h} - H_0^{-,h} \right)
\end{aligned}$$

with $\beta > 0$.

Remark 3.1: The structure of the simultaneous approximation term is similar to the numerical flux in discontinuous Galerkin (DG) methods, in which the parameter γ interpolates between central ($\gamma = 0.5$) and alternating fluxes ($\gamma = 0$ or $\gamma = 1$) and the parameter β adds an upwind component to the numerical flux. In DG methods the choice of numerical flux can have significant effect on the overall accuracy of the method but here, as illustrated in the numerical experiments, the difference between the choices of γ and β is small. This is potentially because the SAT terms only apply at the domain boundary, unlike in DG schemes, the flux terms appear in all cell boundaries.

4) Multiple Dimensions: The generalization of the above procedure to multiple dimensions is straightforward on Cartesian meshes as it can be applied line-by-line in each dimension. Extensions to structured curvilinear meshes is also direct (see, e.g., [19]) but will not be pursued here. Finally, as the nonlinearities we consider here only contain undifferentiated terms, they are naturally handled by the time integrators discussed below.

B. Staggered Summation by Parts Finite Differences

Traditionally SBP finite differences have been restricted to nonstaggered grids but recently O'Reily and coauthors [20], [22] have shown that SBP operators can also be formulated on staggered grids. Given the popularity of the staggered Yee scheme, we also consider discretizations using staggered SBP operators. However, we note that the extension of staggered SBP operators to curvilinear grids is challenging and we will therefore limit the discussion here to 1-D problems.

Define the staggered grids $x_+ = [x_0, x_1, \ldots, x_{n-1}, x_n]$ and $x_- = [x_0, x_{1/2}, \ldots, x_{n-1/2}, x_n]$. On these grids SBP operators, $D_+ \equiv R_+^{-1} Q_+$ and $D_- \equiv R_-^{-1} Q_-$ can be derived, [20]. Again, R_+ and R_- are diagonal matrices and D_+ and D_- approximate the derivatives on the grid x_+ using values from x_- and vice versa. A crucial property of the operators is that they satisfy the SBP identity:

$$Q_+ + Q_- = \left(e_n e_n^T - e_0 e_0^T \right). \tag{12}$$

As above, let $\{E^h, P^h, J^h\}$ and H^h be grid functions approximating $\{E, P, J\}$ and H, on the $-$ and $+$ grids, respectively. We then approximate the derivatives according to

$$\begin{aligned}
E_x &\approx D_- E^h + \sigma_n R_+^{-1} e_n E_n^h + \sigma_0 R_+^{-1} e_0 E_0^h \\
H_x &\approx D_+ H^h
\end{aligned}$$

resulting in the semidiscretization

$$\varepsilon_0 \varepsilon_\infty E_t^h = \left(D_+ H^h - \varepsilon_0 J^h \right) \tag{13a}$$

$$\mu_0 H_t = \left(D_- E^h + \sigma_n R_+^{-1} e_n E_n^h + \sigma_0 R_+^{-1} e_0 E_0^h \right) \tag{13b}$$

$$P_t^h = J^h \tag{13c}$$

$$J_t^h = -J^h/\tau - \omega_0^2 P^h + \omega_p^2 E^h. \tag{13d}$$

To derive a semidiscrete estimate, we multiply (13a)–(13d) by $(E^h)^T R_+$, $(H^h)^T R_-$, $(P^h)^T R_+$, and $(J^h)^T R_+$, respectively, and add them up. Using (12), the discrete energy identity

becomes

$$\frac{1}{2}\frac{d}{dt}\left(\varepsilon_0\varepsilon_\infty (E^h)^T R_+ E^h + \mu_0 (H^h)^T R_- H^h + \frac{\varepsilon_0\omega_0^2}{\omega_p^2}(P^h)^T R_+ P^h + \frac{\varepsilon_0}{\omega_p^2}(J^h)^T R_+ J^h\right) = -\frac{\varepsilon_0}{\omega_p^2\tau}(J^h)^T R_+ J^h + (\sigma_n+1)H_n^h E_n^h + (\sigma_0-1)H_0^h E_0^h.$$

An obvious choice for the penalty parameters is $\sigma_n = -1$ and $\sigma_0 = 1$. This yields an energy conserving discretization when the relaxation time is $\tau = \infty$.

C. Time Discretizations

After semidiscretization in space using SBP operators, the evolution equations take the form of a system of ODEs $y'(t) = f(y(t), t)$, $y(0) = y_0$. This system can be formally solved by integrating in time

$$y(\Delta t) - y_0 = \int_0^{\Delta t} f(y(\tau), \tau)\, d\tau \tag{14}$$

where $\Delta t > 0$ is a suitable time step. The Picard form (14) can be turned into a time-discrete numerical method by approximating the integral using numerical quadrature. This procedure results in implicit Runge–Kutta methods that require the resulting nonlinear system of equations to be solved at each time step. Here we employ the so-called SDC methods [5], on the form analyzed in [6] to iteratively solve these nonlinear equations. This is done at each iteration in which the candidate solution is improved by evolving the correction using the forward Euler method with time steps corresponding to the distance between the quadrature points (note that an implicit or implicit–explicit method could also be used for the correction, see [6] for details). When using a s-point Gauss–Legendre quadrature, it was shown in [6] that the error in the fixed point iteration is accurate to order $2s$ after $2s-1$ corrections. Unless explicitly stated, this is the number of iterations we will use in our numerical computations below. We note that, as the nonlinear system of equations is only solved approximately, the symplectic properties of the Gauss–Legendre Runge–Kutta method will, in general, be lost. Using additional corrections improves the symplectic properties but does not increase the order of accuracy. An advantage with SDC methods compared to explicit Runge–Kutta methods is that they can easily attain high order of accuracy. In addition, since we exclusively use forward Euler for the correction iteration the complexity and implementation of the method is very similar to an explicit method.

Of course as our discretization is of method-of-lines type, other time integrators may also be used. For example, in some of the numerical examples below, we use the classic fourth-order Runge–Kutta method as well as Taylor series.

The constraints on the allowable timesteps depend both on the SBP operator that is used and on the time-stepping method. Typically, increasing the order of accuracy of the SBP operators reduces the timestep slightly while increasing the order of the timestepper increases the allowable timestep linearly with order.

TABLE I
COMPUTED RATES OF CONVERGENCE IN E_x FOR THE PROBLEM DESCRIBED IN SECTION IV-A1

Refinement	1	2	4	8	16	32
L_2-err.	3.7(-2)	3.2(-3)	1.5(-4)	4.5(-6)	3.6(-7)	1.6(-8)
Rate		3.51	4.44	5.03	3.63	4.50

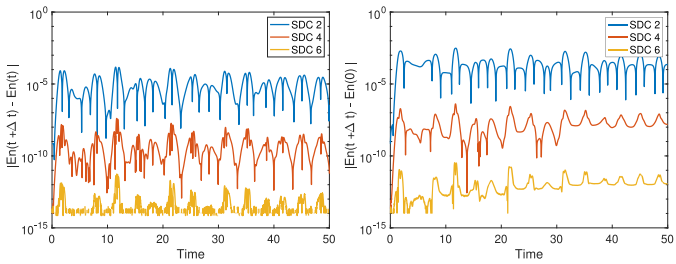

Fig. 2. Left: Difference in energy between subsequent time steps. Right: Drift away from initial energy. Here the notation SDC P refers to a Pth order accurate SDC method with $P/2$ Gauss nodes. Note that the En in the figure refers to energy.

The constraints on the timesteps for the methods we propose are, in general, slightly stricter than those for traditional FDTD.

IV. NUMERICAL EXAMPLES

A. Nonstaggered Discretization in Two Dimensions

In this section, we present numerical examples using nonstaggered SBP operators in two dimensions. To this end, we will use the sixth-order accurate in the interior and third-order accurate on the boundary operator by Strand [17] and choose the free parameter $x_1 = 0.70127127127127$ (defined in [17]). It is known (see, e.g., [1]) that the order of accuracy of this SBP operator is 4 in the L_2 norm. Note that we used normalized units until the very last numerical example.

1) Self-Convergence: To test our method and implementation we perform a self-convergence study for a single material using the PMD model with parameters $\mu_0 = 1.2, \varepsilon_0 = 1.1, \varepsilon_\infty = 1.0, \tau = \infty, \omega_0^2 = 1.5, \omega_p^2 = 1.2, N_{\text{PMD}} = 2, \lambda_0 = 1, \lambda_2 = 1, \lambda_4 = 100$. The computational domain is the square $(x, y) \in [-3/2\pi, 3/2\pi]^2$.

At the initial time all the fields are set to to zero, except H_z which we take to be the trigonometric function

$$H_z(x, y) = \sin(x)\sin(y).$$

We evolve the solution until time $t = 1$ and compute the error in E_x (the other fields have very similar behavior) on a grid with $h = 3\pi/40$ against a reference solution with $h = 3\pi/1280$. To evolve in time we use a sixth-order accurate "explicit" SDC method with Gauss–Legendre nodes with a time step $\Delta t \approx 0.3h$. The results, which can be found in Table I, clearly show that the method is fourth-order accurate.

2) Energy Conservation: We repeat the same computation as in the previous convergence study but set the final simulation time to be $t = 50$ and compare the preservation of the discrete SBP version of the energy $\mathcal{E}(t)$ from (7). In Fig. 2, the difference in energy between two subsequent time steps is

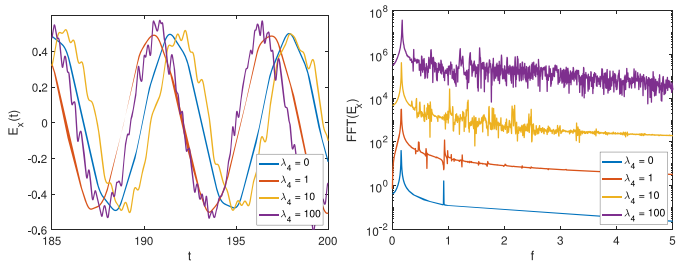

Fig. 3. Left: Time history of the E_x field for the last 15 time units. Right: Spectrum for the different values of λ_4. The upper curves are offset by factors of 100 from the blue curve.

plotted using SDC with 1, 2, and 3 Gauss–Legendre nodes. As discussed above the underlying Gauss–Runge–Kutta methods are symplectic, their SDC approximation is not, and neither is guaranteed to preserve a general energy. This can be observed in Fig. 2 which illustrates that the conservation of energy increases with increasing order of accuracy.

3) Behavior at Longer Times and Stronger Nonlinearity: Next we perform simulations until time $t = 200$, on the same domain as above and with the same initial data but with the material parameters $\mu_0 = 1.2, \varepsilon_0 = 1, \varepsilon_\infty = 1, \tau = \infty,\ \omega_0^2 = 16, \omega_p^2 = 16, \lambda_0 = 1, \lambda_2 = 0$. This corresponds to the linear Lorentz model. We control the nonlinearity by changing λ_4, i.e., by changing to the PMD model with $N_{\text{PMD}} = 2$. Here we are interested in demonstrating the generation of higher harmonics as the nonlinearity controlled by λ_4 is increased according to $\lambda_4 = 0, 1, 10, 100$. To keep the error in the solution small, we use grids with 161^2 gridpoints for the first three values of λ_4, and 321^2 for the last value. We note here that the larger number of gridpoints required for the larger nonlinearity is not due to stability but due to the smaller length and timescales created by the stronger nonlinearity. We also use three Gauss–Legendre nodes in the SDC for the three first values and three nodes for the last. In Fig. 3, we display the E_x field sampled in a point 1/4 along the diagonal from the lower left to the upper right corner. The displayed solution is for the last 15 time units in the computation and for the different values of λ_4. The figure shows how the larger values of λ_4, corresponding to stronger nonlinearity, introduce small oscillations. To quantify this further, we perform a Fourier transform of the signals and plot the spectrum (see Fig. 3).

For the linear model with $\lambda_4 = 0$, there are two primary frequencies, the Duffing (anharmonic) oscillator and the standing mode solution of the free space Maxwell's equations. These are clearly displayed in the blue line in Fig. 3. For the smallest value, $\lambda_4 = 1$, there are only a few new harmonics generated, two of them being in-between the two primary frequencies but for the larger values of λ_4 there is a significant and more uniform generation of harmonics. However, even for the largest nonlinearity, the solution at the final time is very close to a standing mode of the free space problem.

B. Evolution of a Pulse in Different Materials

To demonstrate some different wave propagation behaviors that can be modeled by the Maxwell–Duffing models we consider the evolution of a simple initial data consisting of a magnetic monopole

$$H_z(x, y, 0) = \exp\left(-36(x^2 + y^2)\right).$$

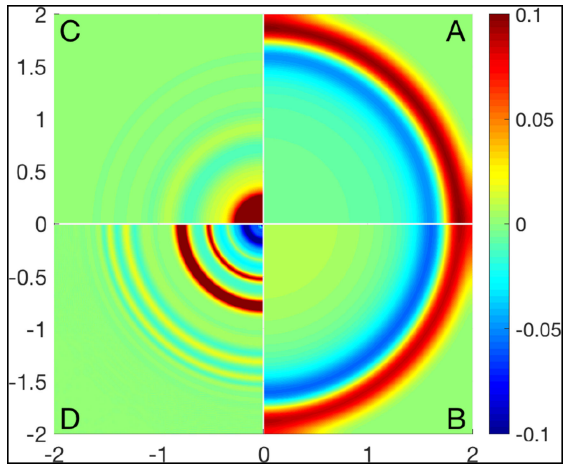

Fig. 4. Outward propagating wave fronts resulting from a magnetic monopole initial data for four different materials.

The computations are performed on a square domain $(x, y) \in [-2, 2]^2$ using a fine grid with $h = 4/500$ and a tenth-order SDC method. The initial data is simulated until time $t = 2$ when we take a snapshot of the H_z field.

The different materials we consider are (A) Maxwell's equations in free space with $\mu_0 = 1.2, \varepsilon_0 = 1, \varepsilon_\infty = 1$, (B) a linear Lorentz dispersive model with $\omega_0^2 = 1, \omega_p^2 = 1$, and $\lambda_0 = 1$, (C) a linear Lorentz dispersive model with $\omega_0^2 = 1, \omega_p^2 = 1000$, and $\lambda_0 = 1$, and (D) a nonlinear PMD model with $\omega_0^2 = 1, \omega_p^2 = 1$, $\lambda_0 = 1$, and $\lambda_4 = 1000$.

In the four quadrants of Fig. 4, we display the solution at the final time for the four different materials. The solution in (A) displays the usual nondispersed outgoing cylindrical shape traveling at speed 1. The main difference between the slightly dispersive solution in (B) and the nondispersive solution in (A) is that there is a slight residue of the initial data in the wake of the wave.

For the material (C), the frequency combination makes the wave essentially nonpropagating with the shape of the solution at the final time being very close to the initial data but with an amplitude that has decreased to 0.75 from 1. If this material becomes nonlinear, as in (D), there are again propagating wavefronts that travel at a much slower speed. In addition the wave fronts are much more concentrated with the larger wave traveling faster than the smaller wave.

In terms of performance, we note that for the solution to above problem, each degree of freedom took around $0.2\ \mu s$ to advance one timestep on a MacBook Pro (2017) with an Intel Core i7 3.5 GHz processor. The code is written in modern Fortran and compiled with `-O3` optimization.

1) Multiblock Method. Self-Convergence: To study the convergence properties for the coupled solver, we simulate Maxwell's equations with material constants set to unity in a domain consisting of three blocks coupled by the interface conditions discussed in Section III, of unit size and with the

TABLE II
SELF-CONVERGENCE OF THE MULTIBLOCK SOLVER FOR MAXWELL'S EQUATIONS IN A NONPOLARIZED MATERIAL WITH $\beta = 0, \gamma = 1$ (TOP), DATA IS FOR $\beta = 0, \gamma = 0.5$ (MIDDLE), AND $\beta = 0.5, \gamma = 0.5$ (BOTTOM)

h	1/20	1/40	1/80	1/160	1/320
L_2-err.	2.28(-2)	5.75(-3)	3.53(-4)	1.03(-5)	6.03(-7)
Rate		1.99	4.03	5.10	4.09
L_2-err.	2.35(-2)	4.95(-3)	2.94(-4)	8.87(-6)	6.61(-7)
Rate		2.25	4.07	5.04	3.75
L_2-err.	2.20(-2)	4.33(-3)	1.81(-4)	7.20(-6)	4.73(-7)
Rate		2.34	4.60	6.65	3.93

TABLE III
SELF-CONVERGENCE FOR A NONLINEAR MODEL. HERE $\beta = 0, \gamma = 0.5$

h	1/20	1/40	1/80	1/160	1/320
L_2-err.	1.58(-2)	4.41(-3)	2.89(-4)	8.45(-6)	5.19(-7)
Rate		1.84	3.93	5.10	4.03

lower left corner of the leftmost block in $(-1, 0)$. The blocks thus occupy the domain $(x, y) \in [-1, 2] \times [0, 1]$. The initial data is taken to be zero for all fields but for H_z which we take to be

$$H_z(x, y, 0) = \exp(-144(x^2 + (y - 0.5)^2).$$

The initial data is evolved for five time units and we compute the error at the final time in the H_z field using a reference solution obtained with $h = 1/640$. We report the L_2 errors for solutions on grids with $h = 1/20, 1/40, 1/80$, and $1/160$. Throughout the experiments with the multiblock method, we use the classic Runge–Kutta method of order four, and in this experiment we set the time step to be $\Delta t = 0.6$ h.

In Table II, we report the errors and the observed rates of convergence (computed as the base 2 logarithm of the ratios of the errors in subsequent grid refinements) for different combinations of γ and β in the SAT. The two uppermost results are for energy conserving ($\beta = 0$) discretizations and would correspond to alternating and central flux in a DG setting. Here, unlike in the DG setting where alternating fluxes typically outperforms central fluxes, the difference between alternating ($\gamma = 1$) and central ($\gamma = 0.5$) averaging is not very pronounced in either the absolute error levels or the rates of convergence. The addition of a slight penalization of a jump at the interface between blocks ($\beta > 0$) also does not appear to impact the overall error levels much.

Finally, in Table III, we repeat the above self-convergence experiment in a nonlinear material with $\omega_0^2 = 16, \omega_p^2 = 16$, and $\lambda_0 = 1$ in all blocks and with $\lambda_2 = \lambda_4 = 1$ and $\lambda_2 = \lambda_4 = 2$ in the middle and rightmost block, respectively, (λ_2 and λ_4 are zero in the leftmost block). The results do not differ much from those obtained in a nonpolarized material confirming that the high order of accuracy of the proposed method also holds in the presence of nonlinearity.

2) Multiblock Domain. A Nonlinear Waveguide: As an example with multiple blocks, we consider a waveguide-like structure occupying the domain $(x, y) \in [0, 5] \times [0, 1]$, which we discretize with five blocks of unit size with Cartesian equidistant grids with grid size $h = 1/400$. Time-stepping is the same as in the previous example. Throughout we set $\mu_0 = \varepsilon_0 = \varepsilon_\infty = 1$ and in the domain $(x, y) \in [2, 3] \times [0, 1]$ we place a material with $\omega_0^2 = 1, \omega_p^2 = 1000, \lambda_1 = 1$, and $\lambda_2 = 10$.

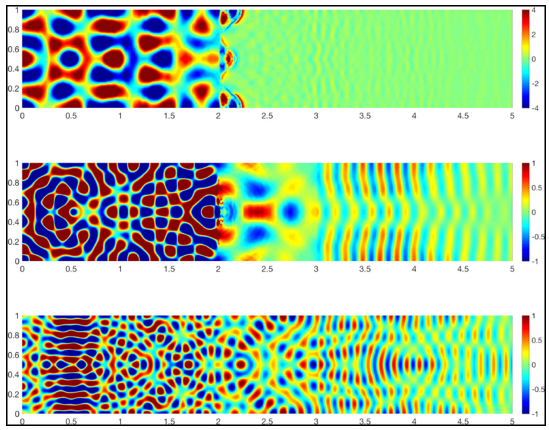

Fig. 5. Snapshots of the magnetic field at time 5. From top to bottom the frequency used in the simulations are 20, 35 and 50.

To illustrate the effect of the nonlinear material for different frequencies, we add the solenoidal forcing

$$\begin{pmatrix} y - 0.5 \\ 0.5 - x \end{pmatrix} 50^2 \sin(\omega t) e^{-200((x-0.5)^2+(y-0.5)^2)}$$

to the evolution equations for equations for $(E_x, E_y)^T$. The simulation is started from rest and we impose PEC boundary conditions on all sides.

In Fig. 5, we display the H_z field at time $t = 5$ for $\omega = 20$, 35, and 50. It is clear that the nonlinear material acts as a pass filter that effectively blocks lower frequencies and allows higher frequencies to propagate. In addition the nonlinear inset appears to make the waves propagate primarily in the x direction.

Even though these simulations have close to a million grid points they run in a few minutes on a serial laptop computer. Rapid simulations with the ability to simulate material interfaces in an accurate, stable and efficient manner opens up the possibility to design multiphysics and multiscale materials and devices via PDE constrained optimization.

C. Staggered Discretization in One Dimension for a Unit-Step Modulated Sine Wave in a Linear Lorenz Medium

As a final example, we perform the experiments depicted in [2, Figs. 3 and 4]. In those experiments, a linear Lorentz model with $\omega_0 = 4 \times 10^{16} \mathrm{rad}/s, \omega_p = \sqrt{20} \times 10^{16} \mathrm{rad}/s, \tau = 0.5/0.28 \times 10^{16} s$ is subject to a unit-step modulated sine wave boundary condition at $x = 0$. In Fig. 6, we display the same data as in [2, Figs. 3 and 4] for a few different grid resolutions with the sixth order. We note that the results agree qualitatively with those in [2] but that there are slight differences. In particular, in the right plot in Fig. 6, we note that the right part of the signal is different. Since [2] does not provide much detail of the simulations, it is hard to assess how accurate the results in [2] are; but as we see grid convergence in our high-order accurate simulations, we have some confidence that they are correct.

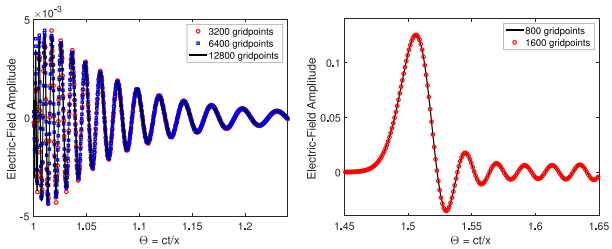

Fig. 6. (Left) The electric field at $x = 1\,\mu$m due a unit-step modulated sine wave with carrier frequency $\omega_c = 10^{16}\,\mathrm{rad}/s$. (Right) The electric field at $x = 10\,\mu$m.

V. Conclusion

In this article, we considered the Duffing models for polarization that incorporate both nonlinearity and dispersion. The general Nth-order polynomial Maxwell–Duffing model has an associated energy estimate that guarantees well-posedness of the continuous model, while including polynomial approximations to an exponential Duffing model and also including the linear Lorentz dispersive model as a special case.

We have presented the construction of novel summation by parts finite-difference time-domain (SBP-FDTD) methods for the numerical discretization of the Maxwell–Duffing models and derived energy estimates for the semi discrete methods that are analogous to the continuous energy estimates. Even though there is no fully discrete energy estimate, our fully discrete methods based on a variety of time integrators have been shown to preserve a general energy-guaranteeing stability of the associated SBP numerical discretizations. In our previous works on energy stable discretizations for Kerr- and Raman-type nonlinearities [4], [14], we showed that the strength of the nonlinearity in the polarization model does not affect fully discrete energy stability. We intend to perform similar analyses for the Duffing models in future research.

The performance of the proposed SBP-FDTD methods were demonstrated in several numerical experiments. There are many avenues for future research. For example, one can investigate nonlinear optical phenomenon such as third harmonic generation. For example, in one of the numerical experiments we observed that even in the presence of strong nonlinearity, coherent structures, like the standing mode we used as initial data, are robust to the nonlinearity.

References

[1] M. Svärd and J. Nordström, "Review of summation-by-parts schemes for initial-boundary-value problems," *J. Comput. Phys.*, vol. 268, pp. 17–38, 2014.

[2] R. M. Joseph, S. C. Hagness, and A. Taflove, "Direct time integration of Maxwell's equations in linear dispersive media with absorption for scattering and propagation of femtosecond electromagnetic pulses," *Opt. Lett.*, vol. 16, no. 18, pp. 1412–1414, 1991.

[3] J. Nordström and R. Gustafsson, "High order finite difference approximations of electromagnetic wave propagation close to material discontinuities," *J. Sci. Comput.*, vol. 18, no. 2, pp. 215–234, 2003.

[4] V. A. Bokil, Y. Cheng, Y. Jiang, and F. Li, "Energy stable discontinuous Galerkin methods for Maxwell's equations in nonlinear optical media," *J. Comput. Phys.*, vol. 350, pp. 420–452, 2017.

[5] A. Dutt, L. Greengard, and V. Rokhlin, "Spectral deferred correction methods for ordinary differential equations," *BIT Numer. Math.*, vol. 40, no. 2, pp. 241–266, 2000.

[6] T. Hagstrom and R. Zhou, "On the spectral deferred correction of splitting methods for initial value problems," *Commun. Appl. Math. Comp. Sci.*, vol. 1, no. 1, pp. 169–205, 2006.

[7] G. Duffing, *Forced Oscillations With Variable Natural Frequency and Their Technical Significance*. Braunschweig, Germany: Vieweg & Sohn, 1918.

[8] I. Kovacic and M. J. Brennan, *The Duffing Equation: Nonlinear Oscillators and Their Behaviour*. New York, NY, USA: Wiley, 2011.

[9] J. Koga, "Simulation model for the effects of nonlinear polarization on the propagation of intense pulse lasers," *Opt. Lett.*, vol. 24, no. 6, pp. 408–410, 1999.

[10] J. H. Greene and A. Taflove, "General vector auxiliary differential equation finite-difference time-domain method for nonlinear optics," *Opt. Exp.*, vol. 14, no. 18, pp. 8305–8310, 2006.

[11] L. Gilles, S. Hagness, and L. Vázquez, "Comparison between staggered and unstaggered finite-difference time-domain grids for few-cycle temporal optical soliton propagation," *J. Comput. Phys.*, vol. 161, no. 2, pp. 379–400, 2000.

[12] V. Janyani, A. Vukovic, J. D. Paul, P. Sewell, and T. M. Benson, "Time domain simulation in photonics: A comparison of nonlinear dispersive polarisation models," *Opt. Quantum Electron.*, vol. 37, nos. 1–3, pp. 3–24, 2005.

[13] J. Kerr, "A new relation between electricity and light: Dielectrified media birefringent," *London, Edinburgh, Dublin Philos. Mag. J. Sci.*, vol. 50, no. 332, pp. 337–348, 1875.

[14] V. A. Bokil, Y. Cheng, Y. Jiang, F. Li, and P. Sakkaplangkul, "High spatial order energy stable FDTD methods for Maxwell's equations in nonlinear optical media in one dimension," *J. Sci. Comput.*, vol. 77, no. 1, pp. 330–371, 2018.

[15] H. Kreiss and J. Lorenz, *Initial-Boundary Value Problems and the Navier-Stokes Equations* (Pure and Applied Mathematics Series), vol. 36, Boston, NY, USA: Academic, 1989.

[16] H.-O. Kreiss and G. Scherer, "Finite element and finite difference methods for hyperbolic partial differential equations," in *Mathematical Aspects of Finite Element in Partial Differential Equations*. New York, NY, USA: Academic, 1974.

[17] B. Strand, "Summation by parts for finite difference approximations for d/dx," *J. Comput. Phys.*, vol. 110, no. 1, pp. 47–67, 1994.

[18] M. H. Carpenter, D. Gottlieb, and S. Abarbanel, "Time-stable boundary conditions for finite-difference schemes solving hyperbolic systems: Methodology and application to high-order compact schemes," *J. Comput. Phys.*, vol. 111, no. 2, pp. 220–236, 1994.

[19] M. Svärd, "Stable high-order finite difference methods for aerodynamics," Ph.D. dissertation, Acta Universitatis Upsaliensis, 2004.

[20] O. O'Reilly, T. Lundquist, E. M. Dunham, and J. Nordström, "Energy stable and high-order-accurate finite difference methods on staggered grids," *J. Comput. Phys.*, vol. 346, pp. 572–589, 2017.

[21] O. O'Reilly and N. A. Petersson, "Energy conservative SBP discretizations of the acoustic wave equation in covariant form on staggered curvilinear grids," 2019, *arXiv:1907.01105*.

[22] K. Mattsson and O. O'Reilly, "Compatible diagonal-norm staggered and upwind SBP operators," *J. Comput. Phys.*, vol. 352, pp. 52–75, 2018.

Daniel Appelö recieved the M.S. degree in electrical engineering and the Ph. D. degree in numerical analysis from the Royal Institute of Technology, Stockholm, Sweden, in 2001 and 2006, respectively.

He is currently an Associate Professor in applied mathematics with the University of Colorado, Boulder, CO, USA.

Vrushali A. Bokil recieved the Ph.D. degree in mathematics from the University of Houston, Houston, TX, USA, in 2003.

She is currently a Full Professor with Oregon State University, Corvallis, OR, USA.

Yingda Cheng recieved the Ph.D. degree in applied mathematics from Brown University, Providence, RI, USA, in 2007.

She is currently an Associate Professor with Michigan State University, East Lansing, MI, USA.

Fengyan Li recieved the B.S. and M.S. degrees in computational mathematics from Peking University, Beijing, China, and the Ph.D. degree in applied mathematics from Brown University, Providence, RI, USA, in 1997, 2000, and 2004, respectively.

She is currently a Full Professor with Rensselaer Polytechnic Institute, Troy, NY, USA.